

Angle-Resolved Photoemission of Topological Matter: Examples from Magnetism, Electron Correlation, and Phase Transitions

Oliver Rader,* Jaime Sánchez-Barriga, Emile D. L. Rienks, Andrei Varykhalov, Gunther Springholz, and Lada V. Yashina

Topological materials promise new functionalities, which are revealed with the help of angle-resolved photoemission. Herein, the search for the magnetic bandgap at the Dirac point as a precondition for the quantum anomalous Hall effect is reviewed and its opening for the topological insulator heterostructure $\text{MnBi}_2\text{Te}_4/\text{Bi}_2\text{Te}_3$ is demonstrated. Essential preconditions are explained and the reasons why nonmagnetic gaps occur when Se replaces Te. Angle-resolved photoelectron spectroscopy (ARPES) probes the quantum mechanical final state, and this allows investigation of spin manipulation by light using spin-resolved ARPES and the dependence of the charge carrier lifetime on the peculiar spin texture of topological states. It is shown that ARPES data do not support Smb_6 as the first strongly correlated topological insulator and an alternative, trivial explanation for the results of ARPES and electrical transport experiments is formulated. Epitaxially grown topological crystalline insulators are, due to their dependence on crystal symmetries, more versatile in the control of individual bulk band inversions. It is shown that this leads to topological quantum phase transitions and associated novel functionalities. Finally, the surface and bulk band connectivity of a type-II 3D Weyl semimetal is investigated and an outlook is given for the scientific field.

1. Introduction

A topological insulator behaves as an insulator in its interior but displays topologically protected metallic states at its surface.^[1–4] This holds for 2D topological insulators, i.e., the quantum spin Hall^[5] and the quantum anomalous Hall insulators,^[6] where backscattering is forbidden and conductance is quantized, as well as 3D topological insulators, where the properties of topological surface states are accessible by angle-resolved photoelectron spectroscopy (ARPES). These edge and surface states are tied to the topologically non-trivial bulk, which is characterized by topological invariants, by the bulk-boundary correspondence. Their predictions, such as the odd number of topological surface states per surface Brillouin zone for a strong topological insulator, can be easily verified by ARPES. This holds also but is a bit more difficult for the bulk bands where the inversion of bands of even and odd symmetry is a precondition for the formation of the topological phase. Topological surface states have a specific spin texture which is characterized by an alignment of spin and linear momentum. This so-called spin-momentum locking is known from Rashba-type surface states,^[7,8] which, however, are topologically trivial. The unique spin texture of topological surface states can be accessed directly by the method of spin-resolved ARPES.^[9]


We studied bulk single crystals and epitaxial films grown by molecular beam epitaxy (MBE). Photoelectron diffraction and holography shows that the surfaces of Bi_2Se_3 and Bi_2Te_3 are chalcogen terminated independently of the method used for the growth.^[10] Also, films grown by metal organic chemical vapor deposition^[11] give high-quality ARPES data.^[12] The stability of the surfaces against ambient conditions has been studied with the result that it requires both oxygen and water to significantly affect Bi_2Se_3 and Bi_2Te_3 ,^[13] while the surface of Sb_2Te_3 oxidizes more rapidly.^[14]

In this topical review, we summarize at first our studies on magnetic topological insulators that are required for the quantum anomalous Hall effect and chiral Majorana zero modes. The main result is the first spectroscopic observation of a magnetic gap at the Dirac point and its connection with a structural modification in magnetically doped topological insulators.

Prof. O. Rader, Dr. J. Sánchez-Barriga, Dr. E. D. L. Rienks, Dr. A. Varykhalov
Elektronenspeicherring BESSY II
Helmholtz-Zentrum Berlin für Materialien und Energie
Albert-Einstein-Str. 15, Berlin 12489, Germany
E-mail: rader@helmholtz-berlin.de

Prof. G. Springholz
Institute for Semiconductor and Solid State Physics
Johannes Kepler Universität
Altenberger Strasse 69, Linz 4040, Austria

Prof. L. V. Yashina
Department of Chemistry
Moscow State University
Leninskie Gory 1/3, Moscow 119991, Russia

 The ORCID identification number(s) for the author(s) of this article can be found under <https://doi.org/10.1002/pssb.202000371>.

© 2020 The Authors. Physica Status Solidi B published by Wiley-VCH GmbH. This is an open access article under the terms of the Creative Commons Attribution License, which permits use, distribution and reproduction in any medium, provided the original work is properly cited.

DOI: 10.1002/pssb.202000371

Subsequently, we discuss lifetime broadening effects peculiar for topological insulators and the role of the light polarization for the spectroscopy. We then address the question whether SmB_6 , the only material seriously considered in experiments as a strongly correlated topological insulator, fulfills the theoretical predictions. Then, we move on to topological insulators protected by crystal symmetries and show that two well-studied systems can, by doping Bi in the bulk, be transformed to a giant Rashba system and to a strong topological insulator protected by time-reversal symmetry. Finally, we discuss a 3D topological phase, the recently predicted type-II Weyl semimetal where the Dirac cones are tilted.

This brief review cannot fully cover the broad topics discussed. The reader is referred to excellent reviews on topological insulators in general,^[1–4] magnetic topological insulators,^[15] samarium hexaboride,^[16,17] topological crystalline insulators,^[18] and Weyl semimetals.^[19]

2. The Quest for the Magnetic Bandgap at the Dirac Point

2.1. The Quantum Anomalous Hall Effect

Among possible applications of topological insulators, those based on the quantum anomalous Hall effect (QAHE) appear particularly within reach. The QAHE features edge states with conductance quantized in units of e^2/h and can be viewed as one-half of the quantum spin Hall effect. While in the quantum spin Hall effect both spin subbands are inverted, in the QAHE, the inversion is modified by the ferromagnetism so that the inversion of one of the spin subbands is released.^[6,20]

There are many possible applications for the QAHE.^[15] One example is lossless interconnects in conventional electronics. Another one is edge state spintronics, which makes use of the spin polarization and of the fact that QAH edge states occur not only at the sample boundary but also around each ferromagnetic domain. Ferromagnetic domains, in turn, can be manipulated optically or by electric currents and in this way the network of edge states, which can represent a spintronics logic circuit, can be modified. In an arrangement of magnetic double layers, these edge states can be switched by the magnetic configuration: *on* for parallel and *off* for antiparallel coupling. The antiparallel coupling gives rise to an axion insulator state. The topological magnetoelectric effect leads to a unique coupling between electric and magnetic properties and can be described by modified Maxwell equations. As a result, an electric field can cause a magnetization and a magnetic field an electric polarization. At interfaces with superconductors, magnetic topological insulators can create chiral Majorana zero modes from the QAH edge states depending on the relative sizes of the superconducting gap induced by proximity and the magnetic gap in the topological insulator. Here, two QAH edge states correspond to one chiral Majorana zero mode, which leads to a half-integer conductance ($0.5e^2/h$), the observation of which has been reported.^[21] A braiding scheme has been suggested and it has been emphasized that readout of qubits may be simpler with the 1D chiral Majorana zero modes as compared to current research efforts with 0D Majorana zero modes.^[22]

This impressive list of possible applications has been propelling the materials science of the QAHE. Starting with a temperature of 30 mK for Cr-doped $(\text{Bi,Sb})_2\text{Te}_3$ in 2013,^[6] the operating temperature of the QAHE has been raised. One strategy aims at improving the magnetic properties by using V instead of Cr, which leads to a $10\times$ higher coercivity.^[23] The other one is to reduce the bulk conductivity.^[24] Yet, the largest increase up to about 1 K has been achieved by a spatially varying dopant concentration, often referred to as delta doping.^[15] The ferromagnetic Curie temperature of these systems is, however, much higher, around 20 to 40 K, which leads to the question what actually keeps the QAHE so far below this fundamental limit.

2.2. Attempts to Observe the Magnetic Bandgap for Surface Impurities

The QAH edge states are accommodated in a magnetic gap at the Dirac point of the surface states. The opening of the gap requires a magnetization and a magnetic anisotropy that is perpendicular to the surface.^[25] It has been predicted that magnetic moments of impurities at the surface of topological insulators such as Sb_2Te_3 are aligned by the RKKY interaction mediated by its topological surface states.^[26] Because for insulating or moderately charge-doped samples the Dirac cone surface state contributes with a very small Fermi surface as compared to the size of the surface Brillouin zone, the sign of the RKKY coupling does not oscillate with the distance between the magnetic impurities and remains ferromagnetic. In addition, the anisotropy is perpendicular to the surface plane.^[26] Based on this prediction, the opening of a magnetic bandgap of ≈ 0.1 eV size was reported for Fe deposited on Bi_2Se_3 .^[27] It was also reported that the Fe provides strong n-type doping and causes Rashba-split surface states to appear.^[27] Interestingly, the Rashba surface state had no gap at its degeneracy point. We investigated this system at room temperature and at low temperature and did not find the opening of a gap at the Dirac point. There were also no Rashba surface states due to n-type doping; on the contrary, Fe deposition at low temperature resulted in p-type doping.^[28] It was concluded that ferromagnetic order with a perpendicular anisotropy was absent in $\text{Fe}/\text{Bi}_2\text{Se}_3$ ^[28] which was confirmed by X-ray magnetic circular dichroism (XMCD).^[29] Ye et al.^[30] subsequently reported perpendicular anisotropy but emphasized that the previous work^[29] was performed at a much lower deposition temperature. The difference was recently clarified based on the accumulation of Fe in the van der Waals gap for room-temperature deposition.^[31]

The absence of a gap means that the Dirac point is robust against disordered magnetic impurities, which we could confirm for a full monolayer of Fe on Bi_2Te_3 .^[32] Also, deposition of Gd ^[33] and Co ^[34] leaves the Dirac cone of Bi_2Se_3 intact. The observed upward shift of the Dirac point^[28] was later observed also for carbon deposition on Bi_2Se_3 and explained by a surface relaxation.^[35]

2.3. The Case of Bulk Impurities and the Nonmagnetic Gap

Two prominent studies reported the opening of an ≈ 0.1 eV large magnetic gap in Bi_2Se_3 caused by incorporation of Fe ^[36] and Mn ^[37] in the bulk. The fact that this occurs even in samples that

do not show long-range ferromagnetic order was explained as an effect of the local magnetic moment of the Fe.^[36] The same problem with Mn was explained by a strongly enhanced Curie temperature at the surface,^[37] which could in principle occur if the topological surface state enhanced the magnetic coupling.^[38] We investigated this case and confirmed the large magnetic gap and its increase with increasing Mn concentration.^[39] Because this gap remains unchanged between 12 K and room temperature, it was regarded as not caused by magnetism^[39] since it has to scale with the sample magnetization.^[38] Even at 1 K, i.e., below the Curie temperature of 6 K, the gap does not increase.^[40] Superconducting quantum interference device (SQUID) measurements show that the magnetization of Mn-doped Bi₂Se₃ is in the surface plane and already therefore incompatible with the opening of a magnetic gap.^[39] To clarify the surface magnetism,^[37] we used XMCD in electron yield. These measurements confirmed that the surface Curie temperature is identical to that of the bulk.^[39]

Because the QAHE has consistently been observed in Cr- and V-doped (Bi,Sb)₂Te₃ samples, one may ask for a spectroscopic observation of the magnetic gap in those systems. Scanning tunneling spectroscopy (STS) did reveal gaps of 20–100 meV in Cr-doped (Bi,Sb)₂Te₃^[41] but these measurements have only been performed for low temperature, so a possible closing of the gap above the Curie temperature could not be investigated.

In fact, a similar gap of ≈ 75 meV was observed in ARPES for Cr-doped Bi₂Se₃ and persisted even at room temperature, i.e., far above the Curie temperature.^[42]

For V-doped Sb₂Te₃, scanning tunneling Landau level spectroscopy has been used to reveal a mobility gap of 32 meV, but this gap was not observable by STS.^[43] It was speculated that the gap cannot be observed in the density of states because of extra V-derived states in the gap.^[43] By ARPES of V-doped (Bi,Sb)₂Te₃, the Dirac point was found to be degenerate with the bulk valence band.^[44] Moreover, a magnetic gap could not be observed when lowering the temperature down to 7 K.^[44] We have recently investigated V-doped (Bi,Sb)₂Te₃ and did not find a magnetic gap down to 1 K.^[45] We found that these bulk-insulating films display a sweep-rate-dependent coercivity and time dependence of the magnetization. We conclude that the loss of magnetization on a time scale of minutes may contribute to the absence of a magnetic gap in ARPES.^[45]

We extended our investigations to the case of impurities where a local magnetic moment can principally not be invoked for a gap opening.^[46] In-doped Bi₂Se₃ is known to lead to a topological phase transition to the trivial phase with increasing In content.^[47] We observed that the gap at the Dirac point opens already at smaller In concentrations than the value for the bulk phase transition of 6%, i.e., it opens within the topological phase.^[46] We studied the behavior of several properties, including the spin polarization of the surface state, and identified the spin–orbit interaction as responsible for the gap opening. In this scenario, the spin–orbit interaction of the Bi₂Se₃ host material is locally lowered by the In impurities because they substitute the heavier Bi atoms. This is sufficient for opening large gaps at the Dirac point, without the need to invoke time-reversal-symmetry breaking.^[46] We have recently adopted this explanation for the nonmagnetic gap of the system Mn in Bi₂Se₃ based on the observation that Mn-doped Bi₂Te₃ does not lead to a nonmagnetic gap at the Dirac point.^[40,48] Bi₂Te₃ has a much larger spin–orbit

interaction than Bi₂Se₃, which is sufficient to protect the Dirac point against the local reduction of the spin–orbit interaction by the incorporation of Mn.^[40]

2.4. First Observation of the Magnetic Gap

Another consequence of the higher spin–orbit interaction in Mn-doped Bi₂Te₃ is the occurrence of perpendicular magnetic anisotropy, as we could recently show.^[40] Experimentally, the perpendicular anisotropy of this system had been known from bulk samples.^[49,50] We studied the behavior of the Dirac cone by ARPES at 1 and 20 K, i.e., below and above the Curie temperature, which is in the range of 10–12 K.^[40] The magnetic gap was at first identified by a broadening at low temperature by 33 meV. Simulations based on this value yielded a large magnetic gap at the Dirac point of 90 meV.^[40] By spin-resolved ARPES at a higher temperature of 6.5 K, a gap of 56 meV was measured directly (**Figure 1**). The spin-resolved data also confirmed the out-of-plane direction of the spin polarization as well as its disappearance at room temperature.^[40]

This size of the gap is unexpectedly large. By density functional theory, a gap of only 16 meV has been predicted for Mn-doped Bi₂Te₃ in which Mn substitutes Bi.^[25] Interestingly, we discovered that there is a structural reason for this discrepancy: Mn incorporation does not primarily lead to Mn substitution of Bi sites as had generally been assumed so far. Instead, the system forms in a self-organized manner an extra Mn–Te (or Mn–Se) bilayer, which is inserted at the center of the quintuple Te–Bi–Te–Bi–Te (or Se–Bi–Se–Bi–Se) layer, transforming it in this way into a septuple layer which has MnBi₂Te₄ stoichiometry and Mn in the center. This modification also explains why Mn incorporation does not affect the charge doping state of the system,^[39] an unresolved question within the scenario of random substitution of Mn²⁺ for Bi³⁺ host atoms. The Mn–Te bilayer is, however, a charge-neutral 2+/2– unit and naturally explains the unchanged charge status of the system.

This Te–Bi–Te–Mn–Te–Bi–Te layer structure is responsible for the large size of the magnetic gap. In a calculation of such a septuple layer of MnBi₂Te₄ placed on top of a Bi₂Te₃ substrate, Otrokov et al. determined an enhancement of the magnetic gap up to 87 meV.^[51] This is five times larger than calculated for the system in which Mn substitutes Bi sites randomly^[25] and is due to the fact that in the layer structure an enhanced overlap of the surface state wave function with Mn-derived states occurs.^[40,51]

The heterostructure system of MnBi₂Te₄/Bi₂Te₃ that permits the observation of the magnetic gap at the Dirac point for the first time is still strongly n-doped and not ready for transport experiments. To confirm the QAHE and push it to higher temperature, the bulk insulating case must be reached. First results show that replacing Bi by Sb is also in this system a promising approach to reach that goal.^[40]

3. Interaction with Light and Lifetime Effects

3.1. Circularly Polarized Light

An important aspect of topological insulators is the time-reversal invariant spin texture of their surface states. As spin-resolved

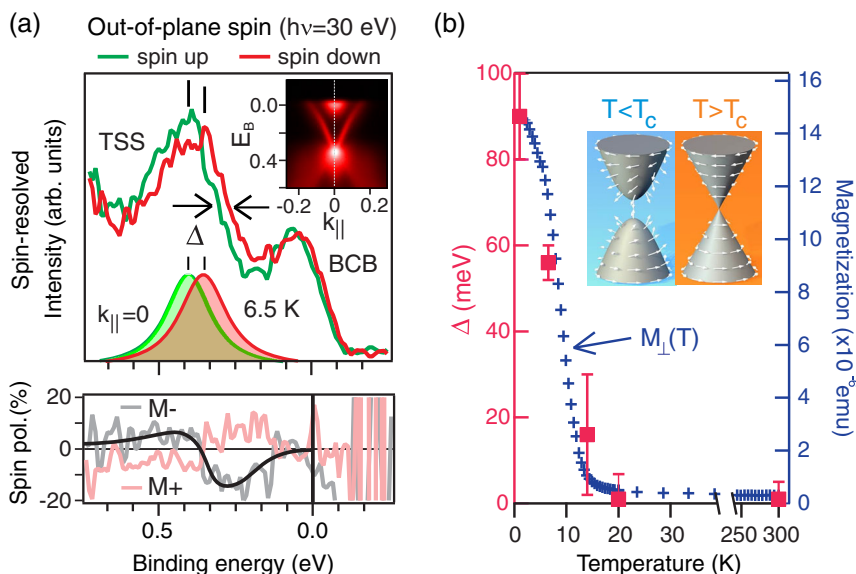


Figure 1. a) Demonstration of the magnetic gap in the magnetic topological insulator heterostructure MnBi₂Te₄/Bi₂Te₃. The upper panel shows spin-resolved ARPES spectra at 6.5 K. The spin quantization axis is perpendicular to the surface. The measured magnetic band gap is $\Delta = 56$ meV at 6.5 K. The inset shows the location of the spin-resolved measurement at the Dirac point. The lower panel shows the spin polarization and its reversal with the magnetization of the sample. b) The magnetic gap from spin-resolved and spin-averaged ARPES measurements follows the macroscopic magnetization of the sample. The inset shows the confirmed spin texture below and above the Curie temperature of ≈ 10 K. Adapted and reproduced with permission.^[40] Copyright 2019, Springer Nature.

measurements are time consuming, there has been the wish to replace them by a more efficient investigation method. In the course of this quest, the circular dichroism in ARPES has been considered. Such an experiment requires only the consecutive measurement of the same ARPES data with circularly positive and circularly negative light polarization and the subtraction of the two signals. The circular dichroism of the Dirac cone of Bi₂Se₃ has been interpreted as showing the initial-state spin angular momentum,^[52] the initial-state orbital angular momentum,^[53,54] and the handedness of the experimental setup.^[55] We could show for the example of Bi₂Te₃ that the circular dichroism depends on the used photon energy and with increasing photon energy changes sign several times.^[56] It is therefore not a measure of the spin texture in the ground state, whereas spin-resolved photoemission with linearly polarized light can be used to determine the spin texture.^[56]

In view of this conclusion that the circular dichroism in ARPES is a final-state effect,^[56] we posed the question how far the combination of both methods, i.e., the excitation of a topological spin texture with circularly polarized light and its detection with spin resolution, would reveal a functional or manipulative effect, in particular in view of possible changes with the photon energy as occur with the circular dichroism.^[56] This became particularly interesting in view of the prediction that, similarly to optical alignment, circularly polarized light will rotate the spins of the Dirac cone in the photoemission process along the propagation direction of the light. The spin orientation can then be reversed by the helicity of the light.^[57]

We conducted the experiment with the Dirac cone surface state of Bi₂Se₃ using at first 50, 60, and 70 eV photon energy, bearing in mind that at 55 eV the largest circular dichroism effect

of 80% appeared for Bi₂Te₃.^[56] For these energies, the in-plane spin orientation as well as the spin polarization of $\approx 50\%$ remained the same, regardless of the light helicity (Figure 2).^[58] Moreover, the spin-resolved spectra were equivalent to those taken with linearly polarized light and independent of the sample geometry in the experiment. The perpendicular spin component was constantly in the range of 10% and did not change with the direction of the linear light polarization or the helicity.^[58] This was in clear contradiction to the theoretical prediction.^[57]

Jozwiak et al. meanwhile took a different approach to this prediction^[57] and used circularly polarized laser light of 6 eV.^[59] They obtained the result that the spin of the photoelectrons of Bi₂Se₃ becomes indeed aligned perpendicular to the sample surface and changes orientation upon reversing the light helicity.^[59] As the first step to understanding the contradiction, we tested our experiment with 6 eV laser light.^[58] We obtained qualitatively the same results as Jozwiak et al. concerning the manipulation of photoelectron spins with circularly polarized light but with the restriction that we could not confirm the high spin polarization value of $\approx 80\%$.^[59] Instead, we found that the value of the spin polarization perpendicular to the sample surface is not very different from the in-plane value of $\approx 50\%$ measured at energies around 50 eV and identified with the ground state (Figure 2).^[58] One may add that also for the spin polarization measured at 50 eV of Bi₂Se₃ different values have been reported of, e.g., 75%.^[60] An experimental factor difficult to control is the apparatus asymmetry of the spin polarimeter; therefore, we repeatedly calibrated our instrument with ferromagnetic samples that allow one to determine this parameter. It has been pointed out that the spin polarization is reduced due to spin–orbit interaction to $\approx 50\%$.^[61] An interesting aspect of the experiment with

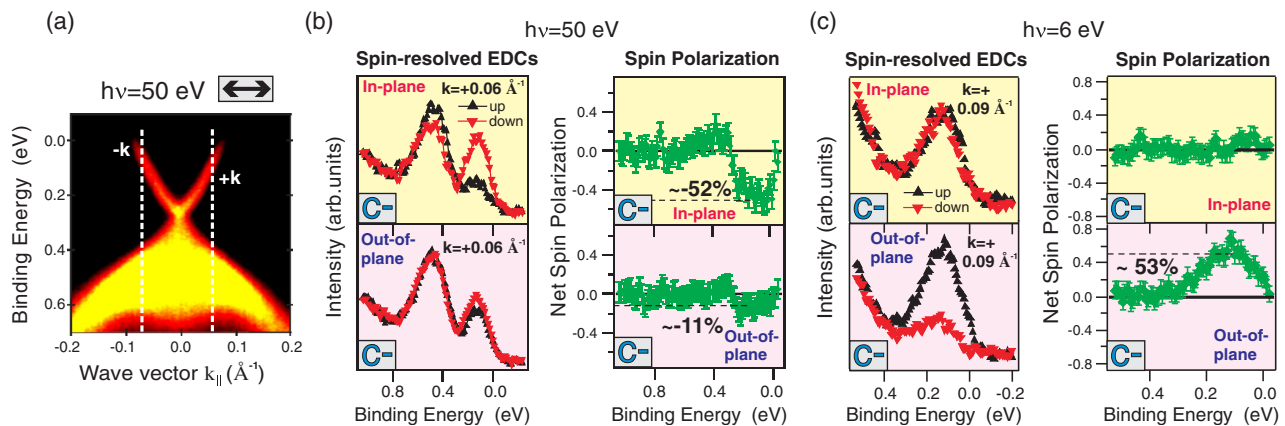


Figure 2. a) The Dirac cone of Bi_2Se_3 measured with linearly polarized light at 50 eV photon energy. Momenta $k_{||}$ for spin-resolved measurements are marked. b) Spin-resolved ARPES from the Dirac cone of Bi_2Se_3 shows that at 50 eV photon energy the spin texture of the ground state is measured, even when circularly polarized light is used. The spin texture is in the surface plane. It reverses with the sign of the momentum $k_{||}$ (see original publication). c) At 6 eV photon energy, the spin turns out of the plane and reverses with the light helicity. It does not reverse with the sign of $k_{||}$. This is explained by the transition into d states in the case of 50 eV and s states for 6 eV photon energy, which is the condition for spin manipulation. Adapted and reproduced with permission.^[58] Copyright 2014, American Physical Society.

6 eV circularly polarized laser light is that it leads to a Dirac cone spin texture of the photoelectrons that would be forbidden in the ground state because it does not obey time-reversal symmetry any longer. As neither the original prediction^[57] nor the publication by the Berkeley group^[59] attributed any role to the photon energy—in fact, a free-electron final state model was used^[57]—we sought for a more refined theoretical model.

A first-principles surface bandstructure calculation coupled to a one-step photoemission calculation^[62] was used to predict the measured spin texture and magnitude of the spin polarization depending on the polarization of the exciting light.^[58] The calculations by Braun et al.^[58] in fact reproduced the different behaviors depending on the photon energy. Moreover, it was possible to clarify the different final states: At 50 eV photon energy, the transition from the Dirac cone, which is made up of p states, occurs primarily into d states. Averaging over the possible transitions gives basically a final-state spin texture that resembles the one of the ground state. At 6 eV, the final state is of s type, which is the precondition for spin manipulation.^[58] This explains nicely why the original prediction^[57] is fulfilled at the laser energy: The free-electron final states correspond to the s-type states in terms of symmetry and, in consequence, either very low photon energies or photon energies as high as several hundred electronvolts are required to achieve spin manipulation. An alternative explanation for the dependence on photon energy and light polarization has been put forward under the assumption of final states of s symmetry.^[63] That approach is largely based on photoelectron interference effects and the predicted layer dependence of the spin texture,^[63] which, however, are both taken into account in our one-step photoemission calculations.^[58]

3.2. Lifetime Broadening

The electron and hole dynamics of topological surface states^[46,64–67] can be affected by their spin texture, which, in turn, is determined by spin–momentum locking. In Bi_2Te_3 , much

more than in Bi_2Se_3 , the surface state is modified by the bulk band structure. The ideally circular shape of the Dirac cone becomes warped into a hexagonal shape.^[68] Berry phase arguments dictate that the spin polarization turns out of the surface plane in some parts of the warped cone,^[68] which could be verified experimentally.^[69] The spin is, however, important for the forbidden backscattering, which holds strictly for 2D topological insulators in the quantum spin Hall effect but at the surface of 3D topological insulators depends on the considered angle.

We analyzed the lifetime broadening of ARPES spectra in Bi_2Te_3 having the following guiding questions in mind. As the hexagonal warping^[68] also enhances nesting properties, it is unclear whether this nesting or the angle dependence of backscattering due to the spin texture of the warped cone will govern possible differences in lifetime. It can be shown that the predictions by these two approaches are discernable as the expected broadening patterns are rotated by 30° .^[64] An assessment requires at first to take the group velocity properly into account. Following the group velocity itself answers the question whether the Dirac cone is warped outward or inward—it is actually warped outward along $\bar{\Gamma}\bar{M}$ (Figure 3) due to the level repulsion between bulk bands and surface states,^[64] an interaction that was not captured properly based on surface-only calculations predicting inward warping.^[68] In particular, we find that neglecting the group velocity reverses the sign of the expected effect or, in other words, rotates the result also by 30° . We could show that it is the spin texture that determines the lifetime broadening (Figure 3).^[64] Scattering rates are low along $\bar{\Gamma}\bar{M}$, i.e., at the tips of the star-shaped constant-energy surfaces and high along $\bar{\Gamma}\bar{K}$, at the waist of the star. This can be explained in the following way: Although the nesting is strong along $\bar{\Gamma}\bar{K}$, the spin texture, which rotates out of the surface plane but remains time-reversal invariant, does not lead to a scattering matrix element along $\bar{\Gamma}\bar{K}$. Taking into account all possible scattering angles, portions with out-of-plane spin of the same orientation will connect and lead to scattering. This result, namely, that the spin dependence causes

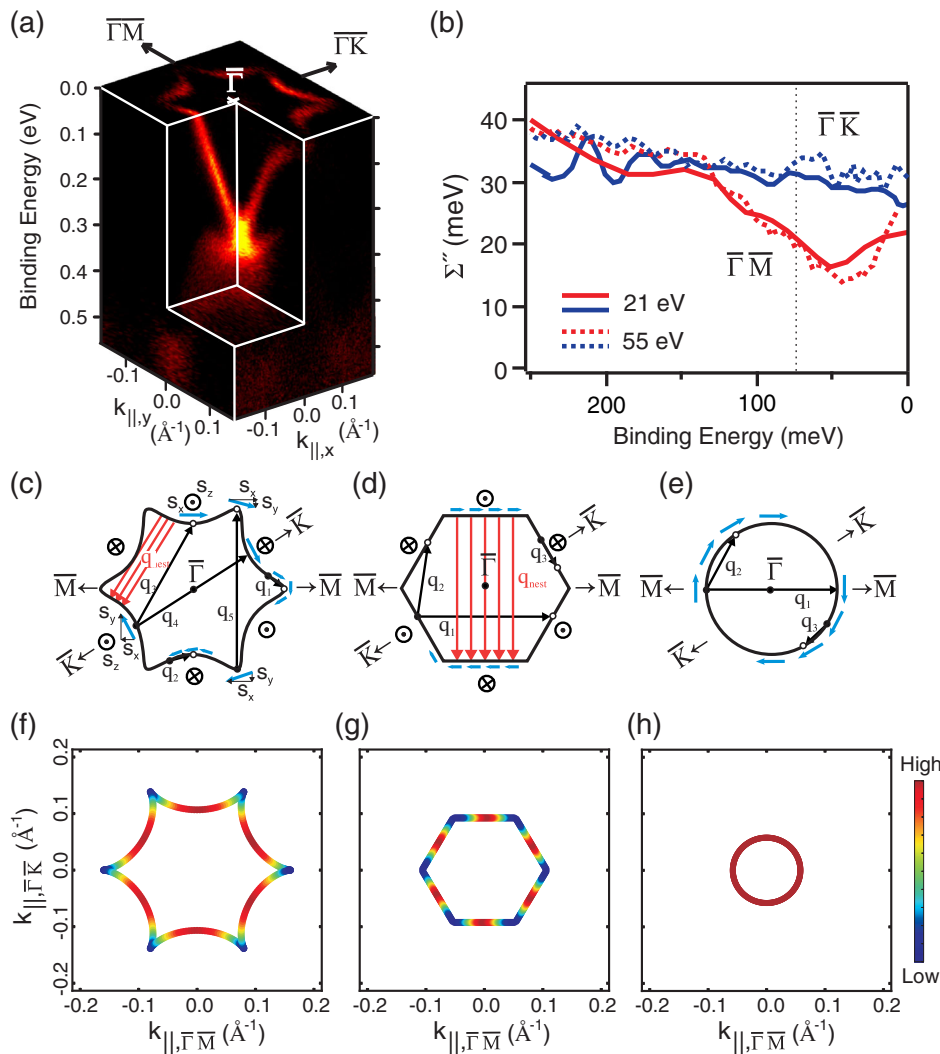


Figure 3. a) The warping of the Dirac cone in Bi_2Te_3 is investigated at 55 eV photon energy. b) The imaginary part of the self-energy depends strongly on the direction but not on the photon energy used. c–e) Schematic of possible scattering channels. The spin texture resulting from the warping is indicated. For energies where the constant energy surface is snowflake-like, the in-plane spin direction changes more strongly with $k_{||}$ in the vicinity of the $\bar{\Gamma}$ – \bar{M} direction as compared to the $\bar{\Gamma}$ – \bar{K} direction. This leads to a smaller probability for small-angle scattering. f–h) A simple model calculation of the scattering amplitude for all \mathbf{q} vectors based on the spin texture describes the experiment well, in contrast to an alternative explanation by nesting [red arrows in (c) and (d)]. Adapted and reproduced with permission.^[64] Copyright 2014, American Physical Society.

the anisotropy of scattering rates, is important for future spintronic devices based on topological insulators.

4. Is Samarium Hexaboride the First Correlated Topological Insulator?

4.1. Topological Kondo Insulators and SmB_6

Although many properties in condensed matter physics depend on electron correlation, topological insulators do not. There are, however, many interesting questions involving the combination of the two, from the stability of topological phases toward strong electron correlation to the emergence of entirely new physics.^[70] From a practical point of view, the achievable inverted bandgaps

of conventional topological insulators are limited to ≈ 0.3 eV. Moreover, systems such as Bi_2Se_3 and Bi_2Te_3 are n-doped and require alloying with Sb and/or Te, Se to become bulk insulating. Mott insulators, on the other hand, achieve large bandgaps due to the Coulomb interaction that are, in addition, centered about the Fermi energy and a hypothetical topological Mott insulator could therefore have practical applications.^[71]

Another important effect driven by strong electron correlations is the Kondo effect. Kondo insulators display bandgaps caused by electron correlation. Here, the energy scales are again rather small. Dzero et al. pointed out that Kondo insulators mix local and itinerant states of opposite parity and can, therefore, give rise to topological insulator phases.^[72] SmB_6 has historically been identified as the first mixed valent compound with a configuration around $4f^{5.5}$.^[73] At low temperature, SmB_6 features

an anomaly in so far as the electrical resistance does not increase further for temperatures below ≈ 4 K, as would have been expected from an insulator, whether ordinary or of Kondo type. Instead, the resistance reaches a plateau,^[74] i.e., a residual metallicity which has for 40 years remained unaccounted for.^[73] The suggestion by Dzero et al.^[72] has at first triggered a reinvestigation of the transport properties, with the result that the residual metallicity could be traced back to the surface of SmB_6 .^[75,76]

4.2. ARPES Results that Seemingly Confirm the Topological Insulator

Experimental investigations of the topological properties of SmB_6 were facilitated by band structure calculations of the (100) surface. Three independent theoretical approaches predicted the odd number of Dirac cone surface states per surface Brillouin zone that are required for a strong topological insulator.^[77–79] Moreover, it was pointed out that, due to the cubic symmetry of SmB_6 , a weak topological insulator phase characterized by an even number of Dirac cones in the surface Brillouin zone cannot exist.^[79]

Subsequently, a number of ARPES studies appeared to confirm the theoretical predictions:^[77–79] Neupane et al.^[80] presented a symmetrized Fermi surface by laser ARPES showing intensity at $\bar{\Gamma}$ as well as contours around \bar{X} , which, however, are much larger than in all subsequent studies. Frantzeskakis et al.^[81] measured contours at \bar{X} but interpreted them as showing a 3D dispersion in experiment, in contrast to all other published studies. They also pointed out that the expected Dirac cone dispersion is missing.^[81] Jiang et al.^[82] also measured the \bar{X} contours as well as intensity at $\bar{\Gamma}$. They also presented circular dichroism in ARPES to conclude on the expected spin texture of the topological surface states.^[82] Denlinger et al.^[83] presented the most detailed investigation of the state at \bar{X} . Xu et al.^[84] measured the Fermi surface contours at \bar{X} and also provided detailed spin-resolved data to support the expected spin texture. Min et al.^[85] also confirmed the Fermi surface contour at \bar{X} . In summary, the measured ARPES data give a very consistent picture of the Fermi surface but could resolve a Dirac cone dispersion neither at $\bar{\Gamma}$ nor at \bar{X} . They were and still are interpreted in support of the topological insulator property of SmB_6 .

4.3. The Surface State at $\bar{\Gamma}$

In our ARPES experiments, we found that the cleavage needed to expose fresh (100) surfaces yields two different well-defined and chemically pure terminations.^[86] These are assigned on the basis of core level shifts of B 1s and Sm 4f spectra. Due to these pure terminations, we could clearly resolve the state at $\bar{\Gamma}$ for the first time. For the Sm termination, the state shows a massive dispersion without any connection to the bulk valence band. This cannot be interpreted as a gapped Dirac cone because for B termination, the state shows a pronounced Rashba-type spin-orbit splitting (Figure 4). This means that the odd number of Dirac cones per surface Brillouin zone cannot be maintained whatever assignment of the \bar{X} state results from the experiment. Moreover, the $\bar{\Gamma}$ state is sensitive to aging of the sample in the residual gas of the experimental chamber and shifts completely

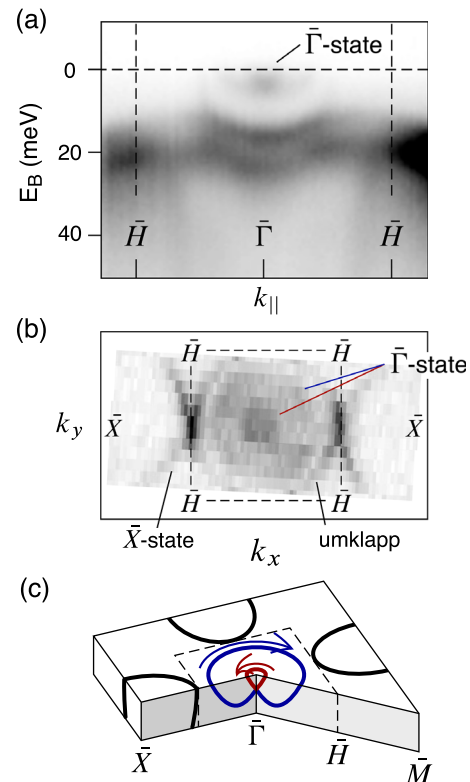


Figure 4. ARPES from boron-terminated SmB_6 . The surface state at $\bar{\Gamma}$ is not a Dirac cone but turns out to be a massive state with Rashba splitting, thus leading to an even number of Dirac cones per surface Brillouin zone. a) Dispersion along $\bar{\Gamma}$ – \bar{H} – \bar{M} . b) Fermi surface where, in addition, an umklapp feature from the surface state at \bar{X} state contributes. c) Overview with the \bar{X} state in black and the $\bar{\Gamma}$ state in blue and red. Adapted and reproduced under the terms of a Creative Commons Attribution License.^[86] Copyright 2018, The Authors, published by Springer Nature.

above the Fermi energy. Both observations lead to the conclusion that the $\bar{\Gamma}$ state is of trivial nature and the ARPES data rather support that SmB_6 is topologically trivial.^[86]

The Rashba splitting, which appears only for the B-terminated surface, is explained by a strong difference in the surface potential gradient between the two terminations.^[86] This difference is indicated by the measured core-level shifts. Due to the very high effective mass in the system ($\approx 17 m_e$), which is a result of the 4f character, a small difference in potential gradient is sufficient for a large Rashba splitting in momentum space. Under different circumstances, the Rashba splitting would have hardly been resolved at the comparatively small Rashba parameter $\alpha_R \approx 3.5 \times 10^{-12}$ eVÅ that we obtain. It should also be mentioned that our measurements of the $\bar{\Gamma}$ state are consistent with the other published ARPES studies. In particular, the massive character of the state can retrospectively be seen in data published by Xu et al.^[87]

4.4. The Surface State at \bar{X}

The closing of the hybridization gap upon increasing the temperature can be observed as ARPES intensity from the bulk

conduction band appearing above the Fermi level.^[83,85] We found its counterpart in the bulk valence band by its temperature dependence and could use this temperature dependence to distinguish bulk from surface bands.^[86] Additional confirmation of the surface character was achieved by sample ageing and the deliberate exposure to oxygen.

In this way we identify two 5d–4f-hybridized dispersions that resemble the calculated bands from Lu et al.^[78] and of which the surface hybrid is shifted by 10 meV to higher binding energy (Figure 5). It is important to be aware of three different energy scales: Divalent and trivalent Sm 4f states differ by several electronvolts. Undercoordinated Sm atoms are shifted by ≈ 0.3 eV. Because the undercoordinated Sm covers the surface, tiny energy shifts of the 5d–4f hybrids of 10 meV can occur below the surface for B as well as for Sm termination. Since the Kondo gap is as small as ≈ 3.5 meV judging from the measured activation energy, energy shifts by 10 meV in either direction will bridge the gap and lead to surface metallicity. Quite expectedly, such shifts appear also for oxygen adsorption, which we studied as a model of a realistic air-exposed surface because transport experiments are performed in air.^[86]

The surface hybrid is not confined to the bulk hybridization gap but is an independent 2D state. This was confirmed by its photon energy dependence. In particular, the 2D character is not at all restricted to the bulk gap region but appears similarly for higher binding energy 4f states. Many more aspects have been treated within the framework of our model such as the mixed valence and the polarity at the surface.^[86]

What could not be resolved is the origin of the reported spin texture.^[84,88] Jiang et al.^[88] used circular dichroism in ARPES to conclude on the spin texture. We have shown for the example of

Bi_2Te_3 , where the spin texture of the Dirac cone is well established, that the circular dichroism is not related to the spin texture.^[56] Concerning the spin-resolved measurements by Xu et al.,^[84] it is possible that it is caused by the Rashba splitting that we observe. On the other hand, it is not resolved why the same group reported a topological spin texture at \bar{X} for the trivial system YbB_6 .^[89]

In summary, our work shows that the surface states at both $\bar{\Gamma}$ and \bar{X} are of trivial nature. The surface metallicity of SmB_6 can be explained by the observed 10 meV energy shifts of the trivial surface state at \bar{X} . These results were at first published in 2015.^[90]

4.5. Support from Scanning Tunneling Microscopy

One of the largest hindrances toward the general acceptance of our results and a possible reason why currently published studies about SmB_6 still consider the system a topological Kondo insulator lies in the inconsistency between ARPES and scanning tunneling microscopy (STM) results. This has been pointed out by Allen in his review.^[16] To give an example, we observe exclusively two chemically pure surface terminations.^[86] On the other hand, a (2×1) reconstruction observed in STM is interpreted as a missing-row reconstruction.^[91,92] This is incompatible with our results because it requires the simultaneous presence of both undercoordinated B and undercoordinated Sm at the surface. All STM studies find (1×1) reconstructed areas.^[91–94] However, Rößler et al.^[92] interpret some (1×1) surfaces as Sm terminated and some (1×1) surfaces as B terminated. Furthermore, they find well-ordered topographies only on small length scales.^[92] Also, Yee et al.^[91] and Ruan et al.^[93] find

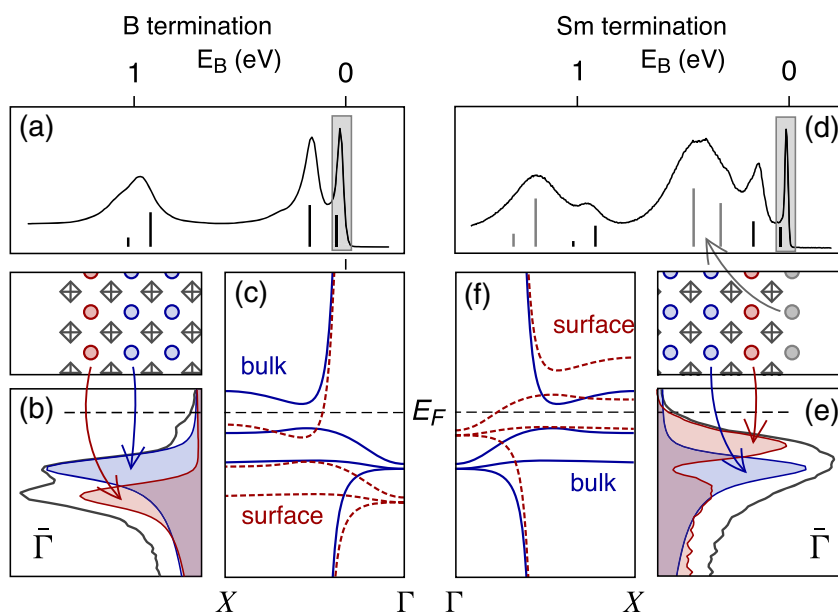


Figure 5. Origin of the \bar{X} surface state for a–c) B termination and d–f) Sm termination. The top row (a,d) shows the divalent 4f multiplet. For boron termination, the 5d–4f hybridized states in (b) are surface shifted to higher binding energy by about 10 meV. For Sm termination, the undercoordinated Sm at the surface is shifted by 0.3 eV in the spectrum (gray arrow). The subsurface Sm in (e) is shifted to lower binding energy by about 10 meV relative to the bulk. c,f) For both terminations, the shifts are large enough to lead to metallic state at the surface as can be seen from calculated bulk bands^[78] after applying corresponding shifts. Adapted and reproduced under the terms of a Creative Commons Attribution License.^[86] Copyright 2018, The Authors, published by Springer Nature.

unstructured areas to be abundant. Because our ARPES data average over a spot size of $\approx 250 \mu\text{m}$, our chemically pure terminations are by many orders of magnitude larger than those reported in STM.

In a combined STM and ARPES experiment involving the same samples, we find that all cleavages are either (2×1) with a peak at -7 meV in STS or (1×1) with less sharp features.^[95] We do find in the literature^[91,92] STS spectra very similar to ours for the (2×1) surface. The same holds for the (1×1) surface,^[91,92] where the STS maximum appears even more pronounced and its location could be determined at -28 meV .^[91] These values agree perfectly with the shifted binding energies that we observe in ARPES for the B-terminated surface (27 meV binding energy) and for the Sm-terminated surface (10 meV binding energy).^[86,95] The STM results are therefore strongly supporting our finding that small binding energy shifts of 10 meV cause the surface metallicity of SmB_6 .

We were also able to determine the possible reason for most of the remaining disagreements. We observe for the (1×1) surface a dependence of the STM image on the bias voltage used. When changing the bias voltage from $+0.2$ to -3.0 V still a (1×1) pattern is recorded, but shifted by half a lattice constant.^[95] We interpret this behavior, which has not been reported before, as due to the fact that the B 2p states appear more than 1 eV below the Fermi energy. These were identified early on in ARPES by Denlinger et al.^[96] and their dispersions were measured in detail for the two terminations.^[86] This means that B states can reliably be imaged only for bias voltages larger than 1 eV , whereas in the literature only very small bias voltages have been used.^[91–94] The fact that the bias-dependent shift in real space is only observed for the (1×1) surface identifies (1×1) as B terminated. The reason is that on the Sm-terminated surface metallic Sm-derived states will likely be picked up for any bias voltage. In addition, we observe vacancies on the (1×1) surface that are only visible for large bias voltages and disappear at small bias. This gives further support to the assignment of the (1×1) surface to B.

In summary, both ARPES and STM support the interpretation of the surface states and surface metallicity of SmB_6 as trivial. The finding that the surface states so far reported by ARPES are trivial is not equivalent to a proof that the bulk band structure of SmB_6 is trivial.^[86] Ideally, the surface shift should be removed at first to gain an unobstructed view at the bulk bandgap of SmB_6 .

5. Doping-Induced Phase Transitions in Topological Crystalline Insulators

5.1. Giant Rashba Effect in $\text{Pb}_{1-x}\text{Sn}_x\text{Te}$

The term “topological crystalline insulators” (TCIs),^[97,98] instead of referring to the crystalline property of the material, means that its topological surface states are protected by crystal symmetries, such as mirror symmetry, rather than by time-reversal symmetry as in conventional Z_2 topological insulators.^[18] In both cases, a bulk band inversion is required, which in prominent TCI materials is well established and can be tuned by composition. $\text{Pb}_{1-x}\text{Sn}_x\text{Te}$ is such a system where the Sn-rich phase is topological.^[99] Its topological phase transition is sensitive to perturbations and can be tuned by different means such as

temperature, pressure, strain, and ferroelectric distortions. Due to their dependence on individual symmetries, the surface states depend on the choice of the surface. Originally, only the (100) surface of cleaved bulk samples had been studied.^[100,101] The (111) surface, on the other hand, presents two different types of surface states. Moreover, it is polar and its preparation requires epitaxial growth.

$\text{Pb}_{1-x}\text{Sn}_x\text{Te}$ is intrinsically p-type due to natural cation vacancies. This tendency increases with higher Sn concentration, which limits the phase diagram for ARPES studies of the Dirac cone surface states. For this reason, we have codoped $\text{Pb}_{1-x}\text{Sn}_x\text{Te}$ by Bi.^[102] The codoping, however, not only successfully moves the chemical potential and allows the ARPES investigation of an extended phase diagram, it also induces a very large Rashba effect of the valence band. This effect does not exist for undoped $\text{Pb}_{1-x}\text{Sn}_x\text{Te}$ and reaches one of the largest Rashba coupling constants ever measured (α_R of 3.8 eV\AA for $\text{Pb}_{0.54}\text{Sn}_{0.46}\text{Te}(111)$ doped with $1\% \text{ Bi}$).^[102] The Rashba effect occurs for systems with broken inversion symmetry in the bulk or at the surface.^[7,8] We could experimentally exclude bulk ferroelectricity as the origin of the effect. Moreover, we used its dependence on the photon energy, i.e., on the electron wave vector component perpendicular to the surface k_\perp , to identify the observed Rashba splitting as a 2D Rashba effect.^[102]

Surface band bending is identified as the origin, caused by acceptor-type trap states at the surface, which lead to upward band bending. This generates a 2D Rashba effect in the valence band. A tight-binding model confirms that the dependence of the Rashba effect on the Bi doping in the bulk is explained by an occupation of the trap states that depends on the bulk Fermi level. A clear proof that the doping dependence is not due to the surface concentration of Bi is achieved by Bi deposition, which does not lead to a Rashba splitting.^[102]

5.2. Topological Quantum Phase Transition in $\text{Pb}_{1-x}\text{Sn}_x\text{Se}$

$\text{Pb}_{1-x}\text{Sn}_x\text{Se}$ has properties similar to those of $\text{Pb}_{1-x}\text{Sn}_x\text{Te}$. Due to the sensitive dependence of the band inversion on the lattice constant, the topological phase transition can be monitored directly in temperature-dependent ARPES experiments.^[103] Also, in this case, the (100) surfaces of single crystals had predominantly been studied. As mentioned above, an important difference of the polar (111) surfaces is that they feature two different surface states, at the $\bar{\Gamma}$ and \bar{M} points, whereas the (100) surface states are located at the \bar{X} points. In both cases, the number of Dirac cones per surface Brillouin zone is even. This distinguishes TCI from Z_2 topological insulators where this number is odd.

When we apply the same strategy of n-doping by Bi in the bulk to extend the range of measurable Sn concentrations (the larger the Sn concentration, the more p-doped the system becomes), we notice that in addition to the desired shift of the Fermi energy, a large bandgap of the order of 0.1 eV opens at the Dirac point at $\bar{\Gamma}$ (Figure 6).^[104] Comparison to the Dirac cones at the \bar{M} points show that these remain gapless. Because there are one $\bar{\Gamma}$ and three \bar{M} points per surface Brillouin zone, the gap means an odd number of intact Dirac cones, which characterizes a Z_2 topological insulator. In other words, the protection has changed

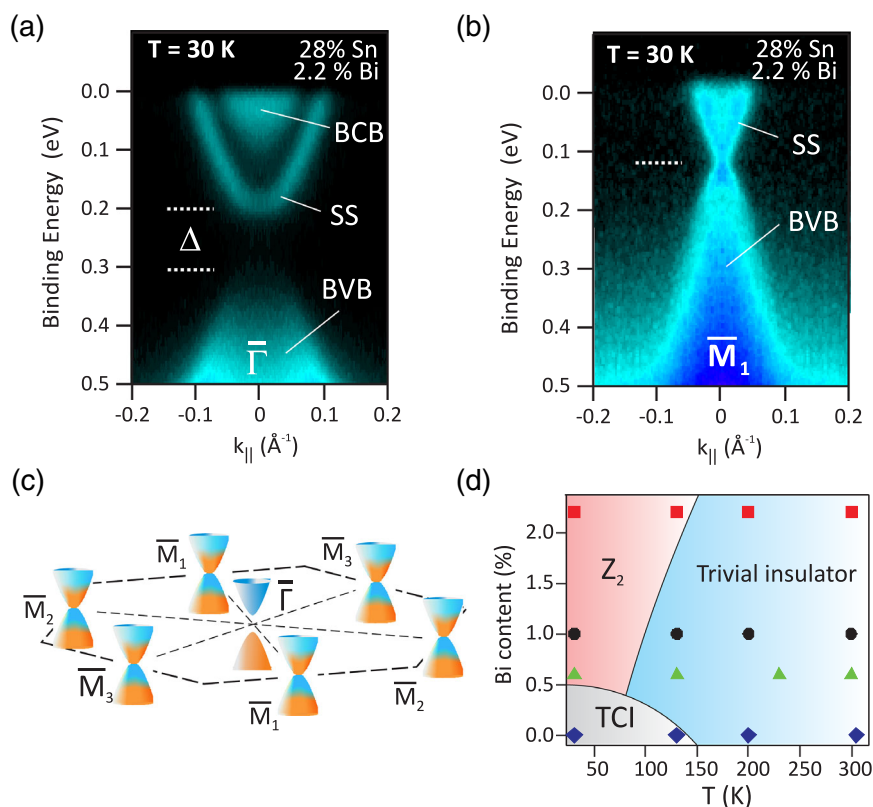


Figure 6. $\text{Pb}_{1-x}\text{Sn}_x\text{Se}$, where 28% Pb is replaced by Sn, is a TCI at low temperature. When the system is doped with 2.2% Bi, a) only the Dirac cone at $\bar{\Gamma}$ opens a gap, whereas b) the Dirac cones at \bar{M} are closed. With three Dirac cones at \bar{M} per surface Brillouin zone, this changes the number of intact Dirac cones from even to odd and the topological phase from topological crystalline to Z_2 topological insulator. Adapted and reproduced under the terms of a Creative Commons Attribution License.^[104] Copyright 2017, The Authors, published by Springer Nature.

from mirror symmetry for the TCI to time-reversal symmetry for the Z_2 topological insulator (Figure 6).^[104] As origin of this topological quantum phase transition, a lattice distortion is identified because for the (111)-oriented films this lifts the fourfold valley degeneracy of the system. The bulk band inversions, which occur at the L points of the bulk Brillouin zone, react differently on a lattice distortion along the [111] surface normal: The L point that projects onto $\bar{\Gamma}$ is much more affected than the specular L points that project onto the \bar{M} points at the border of the surface Brillouin zone.

Because the band inversion can also be tuned by the temperature, two new phase transitions can be observed by ARPES: For the example of $\text{Pb}_{0.72}\text{Sn}_{0.28}\text{Se}$, this is from TCI to Z_2 at low temperature by 0.6% Bi doping and from Z_2 to trivial insulator for 1% Bi by temperature above about 100 K (Figure 6). Interestingly, the underlying lattice distortion is expected to be ferroelectric. This idea, which requires further confirmation by structural investigations at low temperature, holds the promise for electrically switchable topological phase transitions.

6. 3D Weyl Semimetal in a Layered Material

While a topological insulator is a bulk topological phase with a protected Dirac cone in two dimensions, there are topological

phases with Dirac cones in three dimensions.^[19] They can be viewed as originating from an incomplete bulk band inversion that leaves a Fermi surface in only a single point—a 0D one. In 3D Dirac semimetals, the Dirac cones are degenerate due to crystal symmetry. In 3D Weyl semimetals, this degeneracy is lifted by either breaking of inversion^[105] or of time-reversal symmetry.^[106] In both cases, Weyl points of opposite chirality are connected by topologically protected Fermi arcs which are the counterpart of protected surface states of topological insulators. Recently, Weyl semimetals have been classified into type I and type II. Type I is Lorentz invariant and comprises TaAs and related materials. Type II breaks Lorentz symmetry because its Weyl cones are strongly tilted.^[107] This tilt leads to a Fermi surface principally very different from that of type-I Weyl semimetals.

WTe_2 is a material known for its large nonsaturating magnetoresistance^[108] and has been predicted to be such a type-II Weyl semimetal.^[107] WTe_2 is a layered van der Waals material with broken inversion symmetry. We studied the (100) surface obtained by cleavage. Here, we could identify the predicted electron pocket Fermi surface because it shrinks with increasing binding energy as well as the hole pocket, which behaves in the opposite way.^[109] The Weyl points themselves are predicted to lie above E_F and are therefore not detectable by ARPES. However, additional features do not move with changing photon energy and were therefore assigned to surface states or

resonances. Their dispersion with the wave vector parallel to the surface k_{\parallel} distinguishes them further: One surface state connects electron and hole pockets, whereas two features are degenerate with electron and hole pockets.^[109] We concluded that these mediate the coupling between the surface and bulk.

The observed surface resonances are a signature for the expected strong surface–bulk coupling near the Weyl points. Also in In-doped Bi_2Se_3 , the coupling through surface resonances to the bulk plays an important role because it explains how gapped Dirac cones occur on either side of the topological-to-trivial phase transition^[46] and in Sb_2Te_3 , where a kink in the dispersion has been recognized as a sign for the coupling between the Dirac cone and bulk states.^[110] Belopolski et al. discuss different scenarios for the connectivity of the Fermi arcs in $\text{Mo}_x\text{W}_{1-x}\text{Te}_2$.^[111] Bruno et al. had slightly different findings: They identified Fermi arcs in WTe_2 but because these appear only at one out of two possible terminations, they are considered trivial.^[112] Fermi arcs were reported also by Wu et al.^[113] and Wang et al.^[114] The vanishing density of states at the Weyl point makes the chemical potential sensitive to doping. This enabled the observation of a Lifshitz transition by temperature^[115] and by surface doping with potassium.^[116] Despite enormous experimental progress, there are several outstanding issues such as the direct observation of the Weyl points, the clarification of the number of Fermi pockets,^[112,116] and a determination of the length of the Fermi arcs. The spin texture is apparently rather complex but spin polarization in agreement with time-reversal symmetry has been measured for the range of the Fermi arc^[117] and the hole pocket.^[117,118]

7. Conclusion

Topological materials are defined by the connectivity of their band structure. This is investigated theoretically by density functional theory and experimentally by ARPES. In the case of strong electron correlation, the two can deliver very different results as is known from unconventional superconductors, to name an example. This strengthens the role of ARPES and in the current work it was demonstrated that ARPES does not support that Smb_6 is the first strongly correlated topological insulator by showing that the surface states observed in ARPES are of trivial origin.

One might expect that for all other cases of topological insulators, where band structure calculations and ARPES agree very well, the extra insight provided by experiments might be rather limited. The examples shown in the current work emphasize that ARPES experiments are indispensable for verifying the effects predicted under the guidance of band structure theory. Dirac cone warping is a fascinating phenomenon and ARPES clarifies where its effects can be misjudged. Also, the magnetic gap at the Dirac point and its dependence on magnetic anisotropy and temperature, the existence of a nonmagnetic gap and its relation to the spin–orbit interaction could only be clarified by ARPES, with control experiments involving selenides and tellurides. The same holds for lattice distortions in topological crystalline insulators where individual bulk band inversions can be manipulated. Transitions between novel topological phases could be demonstrated. Weyl semimetals pose a particular challenge and require

the ability of ARPES to probe momentum space in three dimensions.

The systems addressed in the current topical review promise a functionalization of topological properties in various ways, e.g., to form quantum anomalous Hall edge states and perform ferroelectric switching of topological phases. With their implementation in devices, ARPES will continue to serve topological materials as an essential investigation method, especially when performed in operando.

Acknowledgements

This work was based on collaborations with many colleagues and the authors acknowledge the contributions by I. Aguilera, G. Bauer, G. Bihlmayer, S. Blügel, J. Braun, O. Caha, A. V. Dukhnenko, H. Ebert, D. Evtushinsky, V. B. Filipov, S. F. Fischer, K. Flachbart, F. Freyse, S. Gabáni, E. Golias, H. Herrmann, P. Hlawenka, O. Kornilov, P. S. Mandal, D. Marchenko, J. Minár, V. S. Neudachina, A. Ney, E. Schierle, M. R. Scholz, N. Shitsevalova, K. Siemensmeyer, M. Sterrer, V. V. Volobuev, A. A. Volykhov, E. Weschke, and many others. This work was supported by the Deutsche Forschungsgemeinschaft (SPP 1666) and the Impuls- und Vernetzungsfonds der Helmholtz Gemeinschaft under Grant Nos. HRSF-0067 and HRJRG-408. The authors gratefully acknowledge financial support from the Russian Science Foundation (RSF) under Grant No. 19-42-06303. Open access funding enabled and organized by Projekt DEAL.

Conflict of Interest

The authors declare no conflict of interest.

Keywords

quantum anomalous Hall effect, quantum phase transition, topological crystalline insulators, topological Kondo insulators, type-II Weyl semimetals

Received: July 7, 2020

Revised: October 25, 2020

Published online: December 2, 2020

- [1] M. Z. Hasan, C. L. Kane, *Rev. Mod. Phys.* **2010**, 82, 3045.
- [2] X.-L. Qi, S.-C. Zhang, *Rev. Mod. Phys.* **2010**, 83, 1057.
- [3] *Topological Insulators* (Eds: M. Franz, L. Molenkamp), Elsevier, Amsterdam/New York **2013**.
- [4] B. A. Bernevig, T. L. Hughes, *Topological Insulators and Topological Superconductors*, Princeton University Press, Princeton **2013**.
- [5] M. König, S. Wiedmann, C. Brüne, A. Roth, H. Buhmann, L. W. Molenkamp, X.-L. Qi, S.-C. Zhang, *Science* **2007**, 318, 766.
- [6] C.-Z. Chang, J. Zhang, X. Feng, J. Shen, Z. Zhang, M. Guo, K. Li, Y. Ou, P. Wei, L.-L. Wang, Z. Q. Ji, *Science* **2013**, 340, 167.
- [7] G. Bihlmayer, O. Rader, R. Winkler, *New J. Phys.* **2015**, 17, 050202.
- [8] A. Manchon, H. C. Koo, J. Nitta, S. M. Frolov, R. A. Duine, *Nat. Mater.* **2015**, 14, 871.
- [9] J. H. Dil, *J. Phys.: Condens. Matter* **2009**, 21, 403001.
- [10] M. V. Kuznetsov, L. V. Yashina, J. Sánchez-Barriga, I. I. Ogorodnikov, A. S. Vorokh, A. A. Volykhov, R. J. Koch, V. S. Neudachina, M. E. Tamm, A. P. Sirotna, A. Y. Varykhalov, G. Springholz, G. Bauer, J. D. Riley, O. Rader, *Phys. Rev. B* **2015**, 91, 085402.

- [11] G. Bendt, S. Schulz, S. Zastrow, K. Nielsch, *Chem. Vap. Deposition* **2013**, *19*, 235.
- [12] G. Bendt, S. Zastrow, K. Nielsch, P. S. Mandal, J. Sánchez-Barriga, O. Rader, S. Schulz, *J. Mater. Chem. A* **2014**, *2*, 8215.
- [13] L. V. Yashina, J. Sánchez-Barriga, M. R. Scholz, A. A. Volykhov, A. P. Sirotnina, V. S. Neudachina, M. E. Tamm, A. Varykhalov, D. Marchenko, G. Springholz, G. Bauer, A. Knop-Gericke, O. Rader, *ACS Nano* **2013**, *7*, 5181.
- [14] A. A. Volykhov, J. Sánchez-Barriga, A. P. Sirotnina, V. S. Neudachina, A. S. Frolov, E. A. Gerber, E. Y. Kataev, B. Senkovsky, N. O. Khmelevsky, A. Y. Aksenenko, N. V. Korobova, A. Knop-Gericke, O. Rader, L. V. Yashina, *Chem. Mater.* **2016**, *28*, 8916.
- [15] Y. Tokura, K. Yasuda, A. Tsukazaki, *Nat. Rev. Phys.* **2019**, *1*, 126.
- [16] J. W. Allen, *Philos. Mag.* **2016**, *96*, 3227.
- [17] L. Li, K. Sun, C. Kurdak, J. W. Allen, *Nat. Rev. Phys.* **2020**, *2*, 463.
- [18] Y. Ando, L. Fu, *Annu. Rev. Condens. Matter Phys.* **2015**, *6*, 361.
- [19] B. Yan, C. Felser, *Annu. Rev. Condens. Matter Phys.* **2017**, *8*, 337.
- [20] R. Yu, W. Zhang, H.-J. Zhang, S.-C. Zhang, X. Dai, Z. Fang, *Science* **2010**, *329*, 61.
- [21] Q. L. He, L. Pan, A. L. Stern, E. C. Burks, X. Che, G. Yin, J. Wang, B. Lian, Q. Zhou, E. S. Choi, K. Murata, *Science* **2017**, *357*, 294.
- [22] B. Lian, X.-Q. Sun, A. Vaezi, X.-L. Qi, S.-C. Zhang, *Proc. Natl. Acad. Sci. USA* **2018**, *115*, 10938.
- [23] C.-Z. Chang, W. Zhao, D. Y. Kim, H. Zhang, B. A. Assaf, D. Heiman, S.-C. Zhang, C. Liu, M. H. W. Chan, J. S. Moodera, *Nat. Mater.* **2015**, *14*, 473.
- [24] A. J. Bestwick, E. J. Fox, X. Kou, L. Pan, K. L. Wang, D. Goldhaber-Gordon, *Phys. Rev. Lett.* **2015**, *114*, 187201.
- [25] J. Henk, M. Flieger, I. V. Maznichenko, I. Mertig, A. Ernst, S. V. Ereemeev, E. V. Chulkov, *Phys. Rev. Lett.* **2012**, *109*, 076801.
- [26] Q. Liu, C.-X. Liu, C. Xu, X.-L. Qi, S.-C. Zhang, *Phys. Rev. Lett.* **2009**, *102*, 156603.
- [27] L. A. Wray, S. Y. Xu, Y. Xia, D. Hsieh, A. V. Fedorov, Y. S. Hor, R. J. Cava, A. Bansil, H. Lin, M. Z. Hasan, *Nat. Phys.* **2011**, *7*, 32.
- [28] M. R. Scholz, J. Sánchez-Barriga, D. Marchenko, A. Varykhalov, A. Volykhov, L. V. Yashina, O. Rader, *Phys. Rev. Lett.* **2012**, *108*, 256810.
- [29] J. Honolka, A. A. Khajetoorians, V. Sessi, T. O. Wehling, S. Stepanow, J.-L. Mi, B. B. Iversen, T. Schlenk, J. Wiebe, N. B. Brookes, A. I. Lichtenstein, P. Hofmann, K. Kern, R. Wiesendanger, *Phys. Rev. Lett.* **2012**, *108*, 256811.
- [30] M. Ye, K. Kuroda, Y. Takeda, Y. Saitoh, K. Okamoto, S.-Y. Zhu, K. Shirai, K. Miyamoto, M. Arita, M. Nakatake, T. Okuda, *J. Phys.: Condens. Matter* **2013**, *25*, 232201.
- [31] M. Chrobak, K. Mackos, M. Jurczyszyn, M. Dobrzanski, K. Nowak, T. Ślęzak, M. Zając, M. Sikora, M. Rams, T. Eelbo, J. Stępień, M. Waśniowska, O. Mathon, F. Yakhou-Harris, D. G. Merkel, I. Miotkowski, Z. Kąkol, A. Kozłowski, M. Przybylski, Z. Tarnawski, *New J. Phys.* **2020**, *22*, 063020.
- [32] M. R. Scholz, J. Sánchez-Barriga, D. Marchenko, A. Varykhalov, A. Volykhov, L. V. Yashina, O. Rader, *Phys. Status Solidi RRL* **2013**, *7*, 139.
- [33] T. Valla, Z.-H. Pan, D. Gardner, Y. S. Lee, S. Chu, *Phys. Rev. Lett.* **2012**, *108*, 117601.
- [34] M. Ye, S. V. Ereemeev, K. Kuroda, E. E. Krasovskii, E. V. Chulkov, Y. Takeda, Y. Saitoh, K. Okamoto, S. Y. Zhu, K. Miyamoto, M. Arita, M. Nakatake, T. Okuda, Y. Ueda, K. Shimada, H. Namatame, M. Taniguchi, A. Kimura, *Phys. Rev. B* **2012**, *85*, 205317.
- [35] S. Roy, H. L. Meyerheim, A. Ernst, K. Mohseni, C. Tusche, M. G. Vergniory, T. V. Menshchikova, M. M. Otrokov, A. G. Ryabishchenkova, Z. S. Aliev, M. B. Babanly, K. A. Kokh, O. E. Tereshchenko, E. V. Chulkov, J. Schneider, J. Kirschner, *Phys. Rev. Lett.* **2014**, *113*, 116802.
- [36] Y. L. Chen, J.-H. Chu, J. G. Analytis, Z. K. Liu, K. Igarashi, H.-H. Kuo, X. L. Qi, S. K. Mo, R. G. Moore, D. H. Lu, M. Hashimoto, *Science* **2010**, *329*, 659.
- [37] S.-Y. Xu, M. Neupane, C. Liu, D. Zhang, A. Richardella, L. A. Wray, N. Alidoust, M. Leandersson, T. Balasubramanian, J. Sánchez-Barriga, O. Rader, *Nat. Phys.* **2012**, *8*, 616.
- [38] G. Rosenberg, M. Franz, *Phys. Rev. B* **2012**, *85*, 195119.
- [39] J. Sánchez-Barriga, A. Varykhalov, G. Springholz, H. Steiner, R. Kirchschlager, G. Bauer, O. Caha, E. Schierle, E. Weschke, A. A. Únal, S. Valencia, M. Dunst, J. Braun, H. Ebert, J. Minár, E. Golias, L. V. Yashina, A. Ney, V. Holý, O. Rader, *Nat. Commun.* **2016**, *7*, 10559.
- [40] E. D. L. Rienks, S. Wimmer, J. Sánchez-Barriga, O. Caha, P. S. Mandal, J. Růžička, A. Ney, H. Steiner, V. V. Volobuev, H. Groiss, M. Albu, G. Kothleitner, J. Michalicka, S. A. Khan, J. Minár, H. Ebert, G. Bauer, F. Freyse, A. Varykhalov, O. Rader, G. Springholz, *Nature* **2019**, *576*, 423.
- [41] I. Lee, C. K. Kim, J. Lee, S. J. L. Billinge, R. Zhong, J. A. Schneeloch, T. Liu, T. Valla, J. M. Tranquada, G. Gu, J. C. S. Davis, *Proc. Natl. Acad. Sci. USA* **2015**, *112*, 1316.
- [42] C.-Z. Chang, P. Tang, Y.-L. Wang, X. Feng, K. Li, Z. Zhang, Y. Wang, L.-L. Wang, X. Chen, C.-X. Liu, W. Duan, *Phys. Rev. Lett.* **2014**, *112*, 056801.
- [43] P. Sessi, R. R. Biswas, T. Bathon, O. Storz, S. Wilfert, A. Barla, K. A. Kokh, O. E. Tereshchenko, K. Fauth, M. Bode, A. V. Balatsky, *Nat. Commun.* **2016**, *7*, 12027.
- [44] W. Li, M. Claassen, C.-Z. Chang, B. Moritz, T. Jia, C. Zhang, S. Rebec, J. J. Lee, M. Hashimoto, D.-H. Lu, R. G. Moore, J. S. Moodera, T. P. Devereaux, Z.-X. Shen, *Sci. Rep.* **2016**, *6*, 32732.
- [45] E. Golias, E. Schierle, T. Flagellari, E. Weschke, E. D. L. Rienks, P. S. Mandal, A. Varykhalov, J. Sánchez-Barriga, F. Radu, N. Samarth, O. Rader, *arXiv:2010.07083*, **2020**.
- [46] J. Sánchez-Barriga, I. Aguilera, L. V. Yashina, D. Y. Tsukanova, F. Freyse, A. N. Chaika, C. Callaert, A. M. Abakumov, J. Hadermann, A. Varykhalov, E. D. L. Rienks, G. Bihlmayer, S. Blügel, O. Rader, *Phys. Rev. B* **2018**, *98*, 235110.
- [47] L. Wu, M. Brahlek, R. V. Aguilar, A. V. Stier, C. M. Morris, Y. Lubashevsky, L. S. Bilbro, N. Bansal, S. Oh, N. P. Armitage, *Nat. Phys.* **2013**, *9*, 410.
- [48] J. Růžička, O. Caha, V. Holý, H. Steiner, A. Ney, G. Bauer, T. Duchon, K. Veltruska, I. Khalakhan, V. Matolin, E. F. Schwier, H. Iwasawa, K. Shimada, G. Springholz, J. New, *Phys.* **2015**, *17*, 013028.
- [49] Y. S. Hor, P. Roushan, H. Beidenkopf, J. Seo, D. Qu, J. G. Checkelsky, L. A. Wray, D. Hsieh, Y. Xia, S.-Y. Xu, D. Qian, M. Z. Hasan, N. P. Ong, A. Yazdani, R. J. Cava, *Phys. Rev. B* **2010**, *81*, 195203.
- [50] M. D. Watson, L. J. Collins-McIntyre, A. I. Coldea, D. Prabhakaran, L. R. Shelford, S. C. Speller, T. Mousavi, C. Grovenor, Z. Salman, S. R. Giblin, G. van der Laan, T. Hesjedal, *New J. Phys.* **2013**, *15*, 103016.
- [51] M. M. Otrokov, T. V. Menshchikova, M. G. Vergniory, I. P. Rusinov, A. Y. Vyazovskaya, Y. M. Koroteev, G. Bihlmayer, A. Ernst, P. M. Echenique, A. Arnau, E. V. Chulkov, *2D Mater.* **2017**, *4*, 025082.
- [52] Y. H. Wang, D. Hsieh, D. Pilon, L. Fu, D. R. Gardner, Y. S. Lee, N. Gedik, *Phys. Rev. Lett.* **2011**, *107*, 207602.
- [53] S. R. Park, J. Han, C. Kim, Y. Y. Koh, C. Kim, H. Lee, H. J. Choi, J. H. Han, K. D. Lee, N. J. Hur, M. Arita, K. Shimada, H. Namatame, M. Taniguchi, *Phys. Rev. Lett.* **2012**, *108*, 046805.
- [54] W. Jung, Y. Kim, B. Kim, Y. Koh, C. Kim, M. Matsunami, S.-I. Kimura, M. Arita, K. Shimada, J. H. Han, J. Kim, B. Cho, C. Kim, *Phys. Rev. B* **2011**, *84*, 245435.

- [55] Y. Ishida, H. Kanto, A. Kikkawa, Y. Taguchi, Y. Ito, Y. Ota, K. Okazaki, W. Malaeb, M. Mulazzi, M. Okawa, S. Watanabe, C.-T. Chen, M. Kim, C. Bell, Y. Kozuka, H. Y. Hwang, Y. Tokura, S. Shin, *Phys. Rev. Lett.* **2011**, *107*, 077601.
- [56] M. R. Scholz, J. Sánchez-Barriga, J. Braun, D. Marchenko, A. Varykhalov, M. Lindroos, Y. J. Wang, H. Lin, A. Bansil, J. Minár, H. Ebert, A. Volykhov, L.V. Yashina, O. Rader, *Phys. Rev. Lett.* **2013**, *110*, 216801.
- [57] C.-H. Park, S. G. Louie, *Phys. Rev. Lett.* **2012**, *109*, 097601.
- [58] J. Sánchez-Barriga, A. Varykhalov, J. Braun, S.-Y. Xu, N. Alidoust, O. Kornilov, J. Minár, K. Hummer, G. Springholz, G. Bauer, R. Schumann, L. V. Yashina, H. Ebert, M. Z. Hasan, O. Rader, *Phys. Rev. X* **2014**, *4*, 011046.
- [59] Ch Jozwiak, C.-H. Park, K. Gotlieb, C. Hwang, D.-H. Lee, S. G. Louie, J. D. Denlinger, C. R. Rotundu, R. J. Birgeneau, Z. Hussain, A. Lanzara, *Nat. Phys.* **2013**, *9*, 293.
- [60] Z.-H. Pan, E. Vescovo, A. V. Fedorov, D. Gardner, Y. S. Lee, S. Chu, G. D. Gu, T. Valla, *Phys. Rev. Lett.* **2011**, *106*, 257004.
- [61] O. V. Yazyev, J. E. Moore, S. G. Louie, *Phys. Rev. Lett.* **2010**, *105*, 266806.
- [62] J. Braun, *Rep. Prog. Phys.* **1996**, *59*, 1267.
- [63] Z.-H. Zhu, C. N. Veenstra, S. Zhdanovich, M. P. Schneider, T. Okuda, K. Miyamoto, S.-Y. Zhu, H. Namatame, M. Taniguchi, M. W. Haverkort, I. S. Elfimov, A. Damascelli, *Phys. Rev. Lett.* **2014**, *112*, 076802.
- [64] J. Sánchez-Barriga, M. R. Scholz, E. Golias, E. Rienks, D. Marchenko, A. Varykhalov, L. V. Yashina, O. Rader, *Phys. Rev. B* **2014**, *90*, 195413.
- [65] J. Sánchez-Barriga, E. Golias, A. Varykhalov, J. Braun, L. V. Yashina, R. Schumann, J. Minár, H. Ebert, O. Kornilov, O. Rader, *Phys. Rev. B* **2016**, *93*, 155426.
- [66] J. Sánchez-Barriga, M. Battiato, M. Krivenkov, E. Golias, A. Varykhalov, A. Romualdi, L. V. Yashina, J. Minár, O. Kornilov, H. Ebert, K. Held, J. Braun, *Phys. Rev. B* **2017**, *95*, 125405.
- [67] J. Sánchez-Barriga, M. Battiato, E. Golias, A. Varykhalov, L. V. Yashina, O. Kornilov, O. Rader, *Appl. Phys. Lett.* **2017**, *110*, 141605.
- [68] L. Fu, *Phys. Rev. Lett.* **2009**, *103*, 266801.
- [69] S. Souma, K. Kosaka, T. Sato, M. Komatsu, A. Takayama, T. Takahashi, M. Kriener, K. Segawa, Y. Ando, *Phys. Rev. Lett.* **2011**, *106*, 216803.
- [70] S. Rachel, *Rep. Prog. Phys.* **2018**, *81*, 116501.
- [71] M. Dzero, V. Galitski, *J. Exp. Theor. Phys.* **2013**, *117*, 499.
- [72] M. Dzero, K. Sun, V. Galitski, P. Coleman, *Phys. Rev. Lett.* **2010**, *104*, 106408.
- [73] E. S. Reich, *Nature* **2012**, *492*, 165.
- [74] J. W. Allen, B. Batlogg, P. Wachter, *Phys. Rev. B* **1979**, *20*, 4807.
- [75] S. Wolgast, Ç. Kurdak, K. Sun, J. W. Allen, D.-J. Kim, Z. Fisk, *Phys. Rev. B* **2013**, *88*, 180405.
- [76] D.-J. Kim, S. Thomas, T. Grant, J. Botimer, Z. Fisk, J. Xia, *Sci. Rep.* **2013**, *3*, 3150.
- [77] T. Takimoto, *J. Phys. Soc. Jpn.* **2011**, *80*, 123710.
- [78] F. Lu, J. Zhao, H. Weng, Z. Fang, X. Dai, *Phys. Rev. Lett.* **2013**, *110*, 096401.
- [79] V. Alexandrov, M. Dzero, P. Coleman, *Phys. Rev. Lett.* **2013**, *111*, 226403.
- [80] M. Neupane, N. Alidoust, S.-Y. Xu, T. Kondo, Y. Ishida, D.-J. Kim, C. Liu, I. Belopolski, Y. J. Jo, T.-R. Chang, H.-T. Jeng, T. Durakiewicz, L. Balicas, H. Lin, A. Bansil, S. Shin, Z. Fisk, M. Z. Hasan, *Nat. Commun.* **2013**, *4*, 2991.
- [81] E. Frantzeskakis, N. de Jong, B. Zwartsenberg, Y. K. Huang, Y. Pan, X. Zhang, J. X. Zhang, F. X. Zhang, L. H. Bao, O. Tegus, A. Varykhalov, A. de Visser, M. S. Golden, *Phys. Rev. X* **2013**, *3*, 041024.
- [82] J. Jiang, S. Li, T. Zhang, Z. Sun, F. Chen, Z. R. Ye, M. Xu, Q. Q. Ge, S. Y. Tan, X. H. Niu, M. Xia, B. P. Xie, Y. F. Li, X. H. Chen, H. H. Wen, D. L. Feng, *Nat. Commun.* **2013**, *4*, 3010.
- [83] J. D. Denlinger, J. W. Allen, J.-S. Kang, K. Sun, J. W. Kim, J. H. Shim, B.-I. Min, D.-J. Kim, Z. Fisk, arXiv:1312.6637v1, **2013**.
- [84] N. Xu, P. K. Biswas, J. H. Dil, R. S. Dhaka, G. Landolt, S. Muff, C. E. Matt, X. Shi, N. C. Plumb, M. Radovic, E. Pomjakushina, K. Conder, A. Amato, S. V. Borisenko, R. Yu, H. Weng, Z. Fang, X. Dai, J. Mesot, H. Ding, M. Shi, *Nat. Commun.* **2014**, *5*, 4566.
- [85] C.-H. Min, P. Lutz, S. Fiedler, B. Y. Kang, B. K. Cho, H. D. Kim, H. Bentmann, F. Reinert, *Phys. Rev. Lett.* **2014**, *112*, 226402.
- [86] P. Hlawenka, K. Siemensmeyer, E. Weschke, A. Varykhalov, J. Sánchez-Barriga, N. Y. Shitsevalova, A. V. Dukhnenko, V. B. Filipov, S. Gabáni, K. Flachbart, O. Rader, E. D. L. Rienks, *Nat. Commun.* **2018**, *9*, 517.
- [87] N. Xu, X. Shi, P. K. Biswas, C. E. Matt, R. S. Dhaka, Y. K. Huang, N. C. Plumb, M. Radovic, J. H. Dil, E. Pomjakushina, K. Conder, A. Amato, Z. Salman, D. M. Paul, J. Mesot, H. Ding, M. Shi, *Phys. Rev. B* **2013**, *88*, 121102.
- [88] J. Jiang, S. Li, T. Zhang, Z. Sun, F. Chen, Z. R. Ye, M. Xu, Q. Q. Ge, S. Y. Tan, X. H. Niu, M. Xia, B. P. Xie, Y. F. X. H. Chen, H. H. Wen, D. L. Feng, *Nat. Commun.* **2013**, *4*, 3010.
- [89] N. Xu, C. E. Matt, E. Pomjakushina, J. H. Dil, G. Landolt, J. Z. Ma, X. Shi, R. S. Dhaka, N. C. Plumb, M. Radovic, V. N. Strocov, T. K. Kim, M. Hoesch, K. Conder, J. Mesot, H. Ding, M. Shi, arXiv:1405.0165v1, **2014**.
- [90] P. Hlawenka, K. Siemensmeyer, E. Weschke, A. Varykhalov, J. Sánchez-Barriga, N. Y. Shitsevalova, A. V. Dukhnenko, V. B. Filipov, S. Gabáni, K. Flachbart, O. Rader, E. D. L. Rienks, arXiv:1502.01542, **2015**.
- [91] M. M. Yee, Y. He, A. Soumyanarayanan, D.-J. Kim, Z. Fisk, J. E. Hoffman, arXiv:1308.1085, **2013**.
- [92] S. Rößler, T. H. Jang, D.-J. Kim, L. H. Tjeng, Z. Fisk, F. Steglich, S. Wirth, *Proc. Natl. Acad. Sci. USA* **2014**, *111*, 4798.
- [93] W. Ruan, C. Ye, M. Guo, F. Chen, X. Chen, G.-M. Zhang, Y. Wang, *Phys. Rev. Lett.* **2014**, *112*, 136401.
- [94] Z. Sun, A. Maldonado, W. S. Paz, D. S. Inosov, A. P. Schnyder, J. J. Palacios, N. Y. Shitsevalova, V. B. Filipov, P. Wahl, *Phys. Rev. B* **2018**, *97*, 235107.
- [95] H. Herrmann, P. Hlawenka, K. Siemensmeyer, E. Weschke, J. Sánchez-Barriga, A. Varykhalov, N. Y. Shitsevalova, A. V. Dukhnenko, V. B. Filipov, S. Gabáni, K. Flachbart, O. Rader, M. Sterrer, E. D. L. Rienks, *Adv. Mater.* **2020**, *29*, 1906725.
- [96] J. D. Denlinger, J. W. Allen, J.-S. Kang, K. Sun, B.-I. Min, D.-J. Kim, Z. Fisk, *JPS Conf. Proc.* **2014**, *3*, 017038.
- [97] L. Fu, *Phys. Rev. Lett.* **2011**, *106*, 106802.
- [98] T. H. Hsieh, H. Lin, J. Liu, W. Duan, A. Bansil, L. Fu, *Nat. Commun.* **2012**, *3*, 982.
- [99] Y. Tanaka, T. Sato, K. Nakayama, S. Souma, T. Takahashi, Z. Ren, M. Novak, K. Segawa, Y. Ando, *Phys. Rev. B* **2013**, *87*, 155105.
- [100] Y. Tanaka, Z. Ren, T. Sato, K. Nakayama, S. Souma, T. Takahashi, K. Segawa, Y. Ando, *Nat. Phys.* **2012**, *8*, 800.
- [101] S.-Y. Xu, C. Liu, N. Alidoust, M. Neupane, D. Qian, I. Belopolski, J. D. Denlinger, Y. J. Wang, H. Lin, L. A. A. Wray, G. Landolt, B. Slomski, J. H. Dil, A. Marcinkova, E. Morosan, Q. Gibson, R. Sankar, F. C. C. Chou, R. J. J. Cava, A. Bansil, M. Z. Hasan, *Nat. Commun.* **2012**, *3*, 1192.
- [102] V. V. Volobuev, P. S. Mandal, M. Galicka, O. Caha, J. Sánchez-Barriga, D. Di Sante, A. Varykhalov, A. Khair, S. Picozzi, G. Bauer, P. Kacman, R. Buczko, O. Rader, G. Springholz, *Adv. Mater.* **2017**, *29*, 1604185.

- [103] P. Dziawa, B. J. Kowalski, K. Dybko, R. Buczko, A. Szczerbakow, M. Szot, E. Lusakowska, T. Balasubramanian, B. M. Wojek, M. H. Berntsen, O. Tjernberg, T. Story, *Nat. Mater.* **2012**, 11, 1023.
- [104] P. S. Mandal, G. Springholz, V. V. Volobuev, O. Caha, A. Varykhalov, E. Golias, G. Bauer, O. Rader, J. Sánchez-Barriga, *Nat. Commun.* **2017**, 8, 968.
- [105] X. Wan, A. M. Turner, A. Vishwanath, S. Y. Savrasov, *Phys. Rev. B* **2011**, 83, 205101.
- [106] A. A. Burkov, L. Balents, *Phys. Rev. Lett.* **2011**, 107, 127205.
- [107] A. A. Soluyanov, D. Gresch, Z. Wang, Q. Wu, M. Troyer, X. Dai, B. A. Bernevig, *Nature* **2015**, 527, 495.
- [108] M. N. Ali, J. Xiong, S. Flynn, J. Tao, Q. D. Gibson, L. M. Schoop, T. Liang, N. Haldolaarachchige, M. Hirschberger, N. P. Ong, R. J. Cava, *Nature* **2014**, 514, 205.
- [109] J. Sánchez-Barriga, M. G. Vergniory, D. Evtushinsky, I. Aguilera, A. Varykhalov, S. Blügel, O. Rader, *Phys. Rev. B* **2016**, 94, 161401(R).
- [110] C. Seibel, H. Bentmann, J. Braun, J. Minár, H. Maass, K. Sakamoto, M. Arita, K. Shimada, H. Ebert, F. Reinert, *Phys. Rev. Lett.* **2015**, 114, 066802.
- [111] I. Belopolski, S.-Y. Xu, Y. Ishida, X. Pan, P. Yu, D. S. Sanchez, H. Zheng, M. Neupane, N. Alidoust, G. Chang, T. R. Chang, *Phys. Rev. B* **2016**, 94, 085127.
- [112] F. Y. Bruno, A. Tamai, Q. S. Wu, I. Cucchi, C. Barreteau, A. de la Torre, S. McKeown Walker, S. Ricco, Z. Wang, T. K. Kim, M. Hoesch, M. Shi, N. C. Plumb, E. Giannini, A. A. Soluyanov, F. Baumberger, *Phys. Rev. B* **2016**, 94, 121112(R).
- [113] Y. Wu, D. Mou, N. H. Jo, K. Sun, L. Huang, S. L. Bud'ko, P. C. Canfield, A. Kaminski, *Phys. Rev. B* **2016**, 94, 121113(R).
- [114] C. Wang, Y. Zhang, J. Huang, S. Nie, G. Liu, A. Liang, Y. Zhang, B. Shen, J. Liu, C. Hu, Y. Ding, *Phys. Rev. B* **2016**, 94, 241119(R).
- [115] Y. Wu, N. H. Jo, M. Ochi, L. Huang, D. Mou, S. L. Bud'ko, P. C. Canfield, N. Trivedi, R. Arita, A. Kaminski, *Phys. Rev. Lett.* **2015**, 115, 166602.
- [116] Q. Zhang, Z. Liu, Y. Sun, H. Yang, J. Jiang, S.-K. Mo, Z. Hussain, X. Qian, L. Fu, S. Yao, M. Lu, C. Felser, B. Yan, Y. Chen, L. Yang, *Phys. Status Solidi RRL* **2017**, 11, 1700209.
- [117] B. Feng, Y.-H. Chan, Y. Feng, R.-Y. Liu, M.-Y. Chou, K. Kuroda, K. Yaji, A. Harasawa, P. Moras, A. Barinov, W. Malaeb, C. Bareille, T. Kondo, S. Shin, F. Komori, T.-C. Chiang, Y. Shi, I. Matsuda, *Phys. Rev. B* **2016**, 94, 195134.
- [118] P. K. Das, D. Di Sante, I. Vobornik, J. Fujii, T. Okuda, E. Bruyer, A. Gyenis, B. E. Feldman, J. Tao, R. Ciancio, G. Rossi, M. N. Ali, S. Picozzi, A. Yazdani, G. Panaccione, R. J. Cava, *Nat. Commun.* **2016**, 7, 10847.



Oliver Rader studied physics in Cologne and obtained his Ph.D. from Free University Berlin. After a postdoctorate at the University of Tokyo, he has been at Helmholtz-Zentrum Berlin, where he heads a department. He is a professor at the University of Potsdam. His research aims currently at the functionalization of graphene and topological insulators with magnetism using synchrotron radiation methods. He coordinates the priority program on topological insulators by the Deutsche Forschungsgemeinschaft.



Jaime Sánchez-Barriga studied at Universidad Autónoma in Madrid and obtained his Ph.D. from the University of Potsdam. He is a staff scientist at Helmholtz-Zentrum Berlin and heads a joint Russian–German research group. His research areas are spin-dependent electronic and dynamical properties of low-dimensional systems and their application in spintronics and optospintronics. He develops time-resolved spectroscopy and microscopy techniques to investigate nonequilibrium phenomena in quantum materials with femtosecond resolution.



Emile D. L. Rienks received his Ph.D. degree from Leiden University, then worked at the Fritz-Haber Institute in Berlin and Århus University. In 2010, he joined the Helmholtz-Zentrum Berlin where, with an intermission at the Leibniz Institute for Solid State and Materials Research and the Technical University Dresden, he has focused on angle-resolved photoelectron spectroscopy. Heavy Fermion materials, in particular in connection to topology, form his main area of interest.



Andrei Varykhalov studied physics at Saint-Petersburg State University. His doctoral research was conducted in Germany at the synchrotron radiation source BESSY, which is now a part of Helmholtz-Zentrum Berlin. He received his Ph.D. degree from the University of Potsdam in 2005. He continued at BESSY as a staff scientist. Currently he leads a group for angle-resolved photoemission and scanning tunneling microscopy at Helmholtz-Zentrum Berlin. His scientific interests are electronic and magnetic properties of novel 2D materials, with particular focus on epitaxial graphene, nanostructures, and topological insulators, as well as development of state-of-the art scientific instrumentation.



Gunther Springholz obtained his Ph.D. from the University of Linz and held research positions at Munich and Leoben. He is a professor at the Institute for Semiconductor and Solid State Physics of the University of Linz. His research deals with compound semiconductors and the growth of semiconductor hetero- and nanostructures with modern epitaxy methods. Current main research topics are the development of optoelectronic components and the investigation of magnetic, electronic, and structural characteristics of multiferroics and topological systems with synchrotron radiation, optical spectroscopy, and scanning probe techniques.



Lada V. Yashina received her Ph.D. in 1996 and habilitation in 2008 in the field of solid-state chemistry of semiconductors and their solid-gas reactions from Lomonosov Moscow State University. She guides the group of surface science and photoelectron spectroscopy of novel materials in the Department of Inorganic Chemistry of the Lomonosov Moscow State University. Her main scientific interests include surface reactivity of carbon materials, including graphene, semiconductors, and topological insulators.